Exp Fluids
DOI 10.1007/s00348-008-0577-2

RESEARCH ARTICLE

# Investigation of the flow in a circular cavity using stereo and tomographic particle image velocimetry

**C. Haigermoser · F. Scarano · M. Onorato**

Received: 14 March 2008 / Revised: 6 October 2008 / Accepted: 7 October 2008


**Abstract** The turbulent flow over a circular cavity with an aspect ratio of $D/H = 2$ is investigated by multi-planar stereoscopic particle image velocimetry and with tomographic particle image velocimetry (PIV). The main aim of the study is the flow topology and the turbulent structure of the asymmetrical flow pattern that forms inside the cavity at these specific conditions. The flow field is measured in the vertical symmetry plane to describe the overall recirculation pattern in the cavity and the turbulent shear layer developing from the separation point. In this specific regime the shear layer fluctuations are recognized as those caused by instabilities together with the effect of the incoming boundary layer turbulence. Additional observations performed at several wall-parallel planes at different height inside the cavity allow to further evaluate the secondary flow circulation generated by this asymmetric regime. The observed flow pattern consists of a steady vortex, occupying the entire cavity volume and placed diagonally inside the cavity such to entrain the external flow from one side, capture it into a circulatory motion and eject it from the opposite side of the cavity. The spatial distribution of the turbulent fluctuations also reveals the same structure. The tomographic PIV measurement returns a visual inspection to the instantaneous three-dimensional structure of the turbulent fluctuations, which at the investigated height exhibit a low level of coherence with slightly elongated vortices in the recirculating flow inside the cavity.

C. Haigermoser (✉) · M. Onorato
Politecnico di Torino, DIASP, Corso Duca degli Abruzzi 24, 10129 Torino, Italy
e-mail: christian.haigermoser@polito.it

F. Scarano
TU Delft, Aerodynamic Section, Aerospace Engineering, Kluyverweg1, 2629HS Delft, The Netherlands
e-mail: F.Scarano@TUDelft.NL

## 1 Introduction

Cavity flows are of high interest in engineering applications, such as wheel wells, fuel vents on aircrafts or cavities between train wagons. In these examples, cavities show to be a considerable acoustic noise source, and especially for increasing Mach number, they can also lead to significant structural loads. It is therefore necessary to understand such flows and find means to control them.

Furthermore, cavity flows exhibit a broad range of fluid mechanical phenomena, like an unsteady shear layer developing from the leading edge, vortex shedding, recirculation zones, instability and 3-dimensional effects. These phenomena play all a role in the cavity flow, even using such a simple geometry.

Generally, cavity flows are categorized upon several characteristics, where the two most important are the geometrical form of the cavity and the upstream boundary layer. Most of the studies up to date have been concerned with rectangular cavity flows and only a few with the flow in a circular cavity.

The scope of this paper is the investigation of the flow in a circular cavity with a diameter to depth ratio $D/H = 2$, where previous studies revealed that the flow in the cavity becomes asymmetric with respect to the streamwise wall-normal symmetry plane of the cavity, which is connected with an increase in drag with respect to other aspect ratios (Dybenko et al. 2006). More precisely, Hiwada et al. (1983) investigated the surface pressure distribution on the cavity walls for aspect ratios

$1 < D/H < 10$ and found the flow being stable and symmetric for $D/H > 5$ and $D/H < 1.25$. Instead for $2.5 < D/H < 5$ the flow becomes unstable and a shear layer flapping was observed. For $1.4 < D/H < 2.5$ the flow becomes asymmetric. This asymmetry was seen to be bi-stable, meaning that it may occur in one or the other direction. Moreover, when the asymmetric flow has already developed, a forced disturbance can change the orientation of this phenomenon.

Dybenko et al. (2006) confirmed these results with surface pressure measurements and hot-wire measurements in the cavity wake. Additionally, they performed acoustic measurements, which revealed a peak in the acoustic spectra for $D/H = 2.12$, which was not present at other aspect ratios. The frequency was close to the one predicted by the Rossiter (1964) formula, whereas the frequencies at the other aspect ratios where well predicted by an equation based on the Helmholtz resonance tone (Sen 1990). Dybenko et al. conclude that the asymmetric flow is somehow related to the occurrence of an acoustic feedback mechanism.

Rona (2007) developed an analytical model to investigate oscillations in circular cavities. At aspect ratios of 0.71 and 2.5 asymmetric flow modes were predicted, where only the prediction for the latter aspect ratio corresponds to the experimental investigations of Hiwada et al. (1983) and Dybenko et al. (2006). As it was shown experimentally by Hiwada (1983) and Dybenko et al. (2006), Rona (2007) predicts the asymmetric modes being oriented in one or the other direction.

The mentioned studies of cylindrical cavity flows confirm the occurrence of a asymmetric 3-dimensional flow pattern inside the cavity, but a direct measurement of the flow field is still missing, due to the point measurement techniques applied in previous studies. Therefore, the scope of this study is clarify this flow pattern using stereoscopic and tomographic PIV.

## 2 Experimental setup

The experiment was conducted at the Aerodynamics Laboratories of TU Delft in a open wind tunnel with a test section area of 400 × 400 mm$^2$. A flat plate was placed upstream of the cavity to control the development of the upstream boundary layer, which was tripped at the flat plate's leading edge with a strip of sand paper. The plate was placed into the test section center and the cavity was situated right at the test section exit in order to enable optical access (see Fig. 1). The cavity's aspect ratio was $D/H = 2$. The coordinate system has the $x$-axis originating from the cavity's leading edge in the streamwise-wall-normal symmetry plane (Fig. 1).

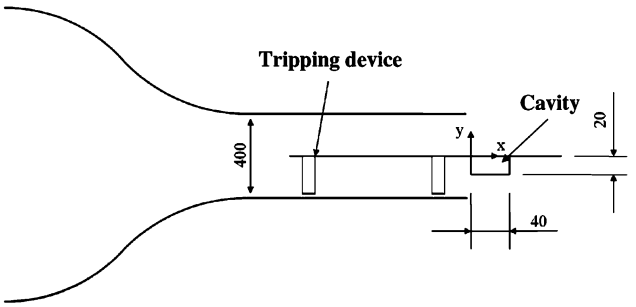


**Fig. 1** Experimental setup; units in mm; cavity not in scale

The cavity's upstream boundary layer was fully turbulent with the characteristics as shown in Table 1. The ratio of the boundary layer thickness and the cavity depth was $\delta/H = 1.125$ and was deemed to be large to produce a regular vortex shedding due to shear layer instabilities (see Grace et al. 2004). An important parameter which determines the occurrence of oscillations in a cavity is the ratio of the cavity length (respectively diameter) $D$ over the boundary layer momentum thickness $\theta$. This ratio is here 14, which is low with respect to values found in literature for rectangular cavities, above which cavity flow oscillations are expected (see Grace et al. 2004). These experimental conditions were chosen to be as similar as possible to the ones of Dybenko et al. (2006) to maximize the possibility to reproduce the reported asymmetric flow pattern. Moreover, it was attempted to produce a model and a setup as clean and symmetric as possible in order to exclude initial asymmetric conditions, which could lead to a forced asymmetry in the flow.

The experiments were conducted by using 2 (for stereo PIV) and 4 (for tomographic PIV) PCO Sensicam QE CCD cameras (1,376 × 1,040 pixels). The cameras were equipped with Nikon lenses with a focal length of 60 mm at f♯ = 8. The measurement plane, respectively the measurement volume, was illuminated by BigSky CFR200 Nd:YAG laser with a maximum energy of 200 mJ per pulse and a maximum repetition rate of 30 Hz. Oil droplets with a diameter of 1 μm were used to seed the flow, yielding a particle image diameter of approximately 3 pixels.

Before correlating the images, a background image was subtracted from the PIV images to reduce reflections coming from the cavity walls. Three kinds of experiment were carried out:

**Table 1** Incoming boundary layer characteristics

| $U_e$ (m/s) | $\delta$ (mm) | $\theta$ (mm) | $Re_L$ | $D/\theta$ | $\delta/H$ |
|---|---|---|---|---|---|
| 12 | 22.5 | 2.8 | 31,000 | 14 | 1.125 |

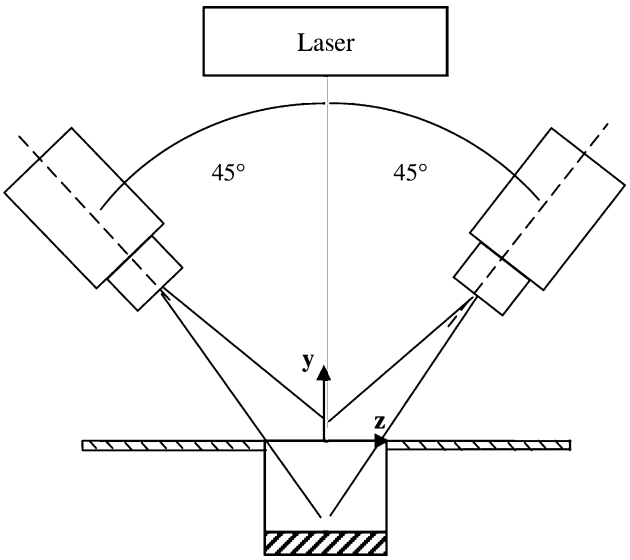


**Fig. 2** Stereo PIV setup in vertical plane

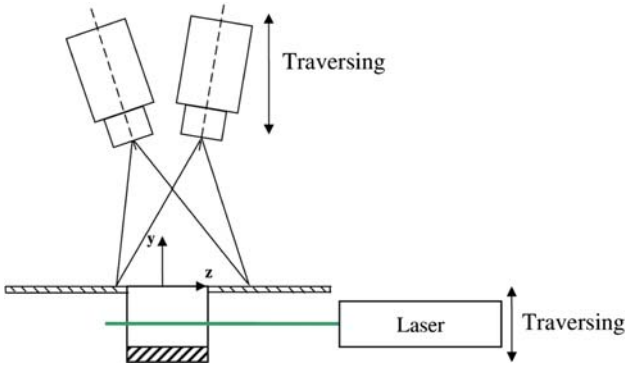


**Fig. 3** Stereo PIV setup in horizontal planes

(a) Stereo PIV measurements in the vertical streamwise ($x$–$y$) plane in the middle of the cavity (Fig. 2).
(b) Stereo PIV measurements in different horizontal stream wise ($x$–$z$) planes, placed at different heights along the cavity axis (Fig. 3).
(c) Tomographic PIV measurements in the upper half of the cavity.

For the stereo PIV measurements in the vertical plane, the two cameras were placed as shown in Fig. 2. The laser light sheet illuminated the streamwise wall-normal ($x$–$y$) plane in the center of the cavity (see Fig. 2). The field of view covered the whole cavity and the outer flow ($-20$ mm $< x <$ 20 mm; $-20$ mm $< y <$ 20 mm). The images were analyzed with the LaVision Davis 7.3 software, using a multi-step cross-correlation with a final interrogation window size of $32 \times 32$ pixels ($0.9 \times 0.9$ mm$^2$) with 50% overlap. The datasets used for statistical evaluation comprised 800 statistically independent snapshots.

For the stereo PIV measurements in the horizontal planes, the two cameras were placed above the cavity with an angle of 10° with respect to the cavity axis, and they were fixed onto a vertically traversing rigid structure. The camera angles are low to maximize the field of view, higher angles would have increased the accuracy of the out-of-plane component (Fig. 3). The field of view was $60 \times 44$ mm$^2$ and included the cavity and a part of the flow downstream of it.

The laser light sheet was introduced laterally through the cavity side walls, which made it necessary to build them as thin as possible, in order to minimize the refraction of the light sheet and to insure a homogeneous illumination of the particles inside the cavity (Fig. 3). The measurements were performed at 12 different wall-normal positions spaced between $-0.85H < y < 0.4H$, by moving the laser and the cameras along the wall normal direction.

The images were cross correlated using the same type of algorithm as in the vertical stereo measurements, see above. Here, one vector represents the mean velocity in a area of $1.4 \times 1.4$ mm$^2$. At each location 300 statistically independent instantaneous velocity fields were obtained.

The stereoscopic system was calibrated outside the cavity with a 2-level calibration target and the calibration was corrected at each level using a self-calibration procedure, see Wieneke (2005). The error in measuring the particle displacement with the vertical PIV setup is estimated to be about 0.1 pixels due to the good image quality, image preprocessing and the application of a self-calibration procedure. Therefore, the error in measuring the in-plane velocity components can be estimated to be about 1% at a particle displacement of about 10 pixels in the shear layer. The error increases for the out-of plane component as the displacement of the particles is much less. It is estimated to be in the order of 2-3% and even larger for the horizontal stereo PIV setup, where the viewing angle of the cameras is only 10°. Consequently, also the error in measuring the velocity rms values is the same as the error in measuring the respective velocities.

The tomographic PIV experiment was carried out adding two cameras to obtain a total of four views all inclined 10° from the cavity axis. The laser light sheet was expanded to a thickness of 8 mm. The measured volume was located at $-0.5H < y < -0.1H$.

The images were pre-processed subtracting the background using images captured without introducing any seeding. Further, the particle image intensity was equalized and pixel noise was reduced by Gaussian smoothing.

The volumes were reconstructed using six MART iterations (see next section) at a pixel to voxel ratio of 1, leading to a volume of $1{,}094 \times 1{,}088 \times 224$ voxels (24 voxels/mm). The reconstructed volumes were cross-correlated using the VODIM software developed at the TU Delft.

The final interrogation volume size was 30 × 30 × 30 voxels (1.6 × 1.6 × 1.6 mm$^3$) at an overlap of 50%. The error of a tomographic PIV setup was assessed by Elsinga et al. (2006), where the displacement error is estimated to lie between 0.1 and 0.16 voxels. It is mentioned that this error can still be improved applying a self-calibration procedure, as it was done in the present case. Anyway, considering the above error level, the error in measuring the velocity in the present case can be estimated to be lower than 2% at a displacement of the particles of about 10 voxels within an image pair inside the shear layer.

## 3 Tomographic PIV-working principle

This section gives a quick overview on tomographic PIV. For details one is referred to Elsinga et al. (2006) and Elsinga et al. (2006). The working principle is shown in Fig. 4 [figure from Elsinga et al. (2006)]. A fluid volume seeded with particles is illuminated with a thick laser light sheet. Two successive images are recorded simultaneously with four cameras as it is done in stereo PIV. In the successive step one has to obtain the 3D distribution of the particles in the volume from the four images. Here comes in the new part of the technique, the tomographic reconstruction. It was seen that an algebraic iterative algorithm was most appropriate for the reconstruction. The multiplicative algebraic reconstruction technique (MART) assumes a light intensity distribution

$E(X,Y,Z)$ divided in voxels and relates it to the pixel intensity $I(x,y)$ obtained from the cameras via a weighting factor $w_{i,j}$

$$\sum_{j\in N_i} w_{i,j}E(X_j,Y_j,Z_j) = I(x_i,y_i) \tag{1}$$

where the index $i$ refers to the camera pixels and $j$ refers to the voxels in the volume. The voxel intensity $E(X,Y,Z)$ is updated in every iteration:

$$E(X_j,Y_j,Z_j)^{k+1} = E(X_j,Y_j,Z_j)^k \left( \frac{I(x_i,y_i)}{\sum_{j\in N_i} w_{i,j}E(X_j,Y_j,Z_j)^k} \right)^{\mu w_{i,j}} \tag{2}$$

where $\mu$ is a scalar relaxation parameter, which for MART must be $\leq 1$. Having obtained the 3D light distribution a 3D cross-correlation algorithm is used to calculate the velocity vectors in the volume, similar to a 2D cross-correlation.

The time to obtain one reconstructed volume was approximately 1 h on a quad-core PC. The 3D correlation required about the same time.

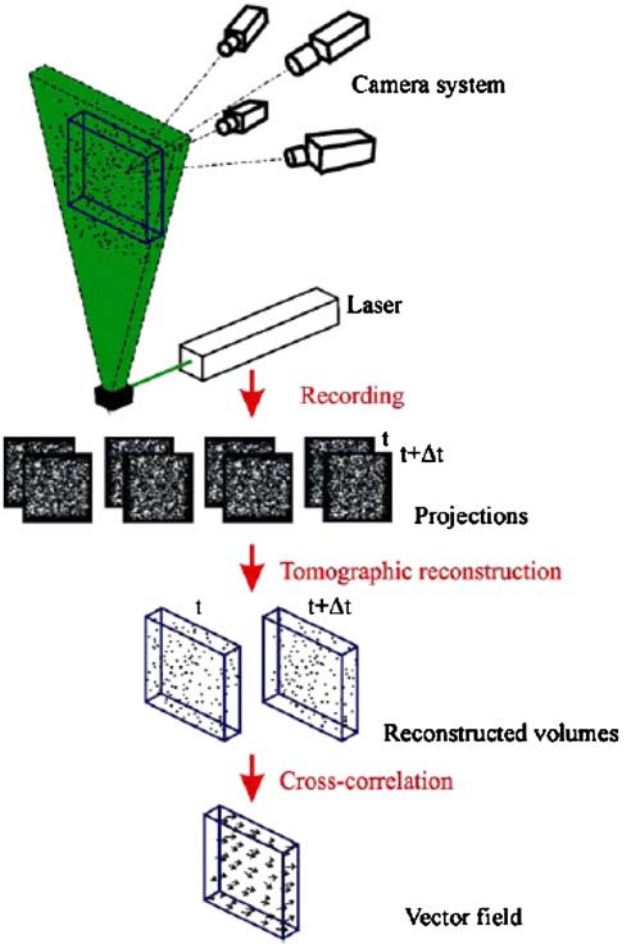


**Fig. 4** Working principle of tomographic PIV. Figure from Elsinga et al. (2006)

## 4 Stereo PIV results

### 4.1 Vertical plane

The mean velocity field from the measurements in the vertical symmetry plane (Fig. 5) shows a recirculation zone occupying the whole cavity. The asymmetry of the flow is indicated by the out of plane velocity component. One notices the flow going in positive z direction close to the upper corner at the cavity's leading edge and going in negative $z$-direction close to the bottom at the trailing edge. Moreover, in the middle of the cavity mouth respectively in the shear layer, the spanwise velocity component shows to be positive. Thus, the asymmetric motion in the cavity is strong enough to influence the zones of high momentum in the shear layer. This strong asymmetric motion and the respective entrainment of the flow into the cavity lead to a strong increase of drag with respect to symmetric circular cavity flows (Dybenko et al. 2006). Figure 6 shows a plot

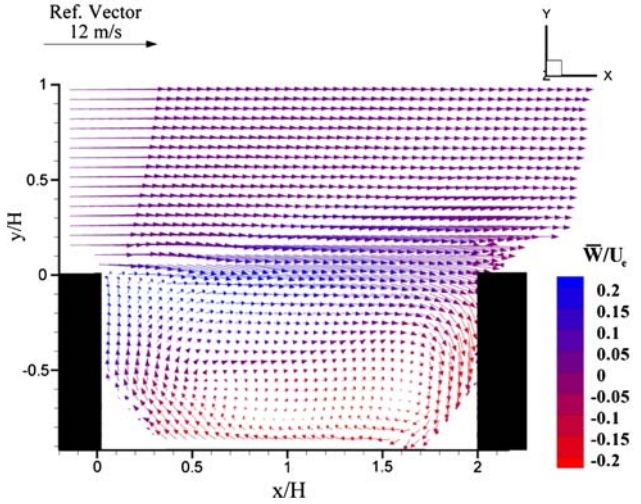


**Fig. 5** Mean velocity field in the plane of symmetry; vector color coded by out of plane mean velocity component $\overline{W}/U_e$

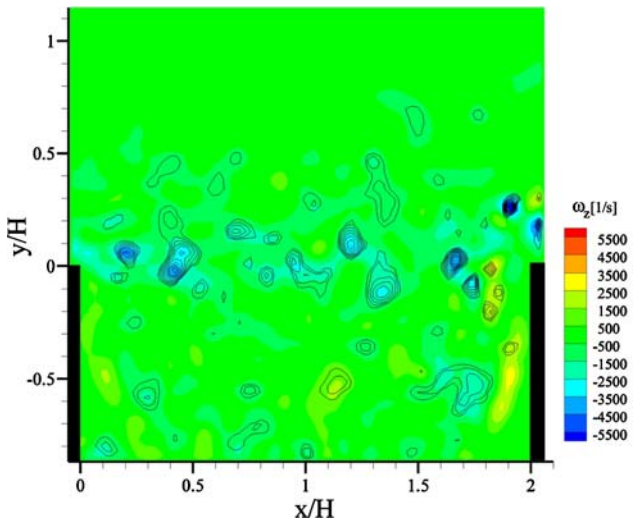


**Fig. 6** Instant flow field. Color plot: Vorticity $\omega_z$; isolines: $\lambda_{ci}$

of the instant vorticity $\omega_z$ and $\lambda_{ci}$ isolines identifying vortices (Zou et al. 1999). The vorticity was obtained, calculating the velocity derivatives, performing a least square fit to a 2-dimensional second order polynomial function with a kernel size of 5 × 5 grid points. Based on this data also the $\lambda_{ci}$ values were obtained, see (Zou et al. 1999). As expected because of the low $D/\theta$ ratio, an irregular vortex shedding is seen from the leading edge. For regular vortex shedding the flow pattern would show a more regular spacing of the vortices in the shear layer. Apparently, due to the thick boundary layer, the shear stresses in the shear layer are not high enough to induce regular instability mechanisms. Instead, it is assumed that the flow structures of the incoming boundary layer dominate the shear layer instability mechanism. It must be pointed out that these observations are only based on a qualitative observation of the flow and to clearly determine weather the vortex shedding is regular or not, time-resolved data would be necessary.

In Fig. 7a–c the RMS values of the three fluctuating velocity components normalized with the free stream velocity $U_e$ are shown. In all figures a similar pattern is observed, which is also known from rectangular cavity flows (see e.g. Haigermoser et al. 2008; Ukeiley and Murray 2005). Downstream, the fluctuations grow in amplitude and the region spreads in wall-normal direction. The maximum of the normalized RMS values for the $U$ and $V$ component is found at $x/H \approx$ 1.25 with values of 0.07

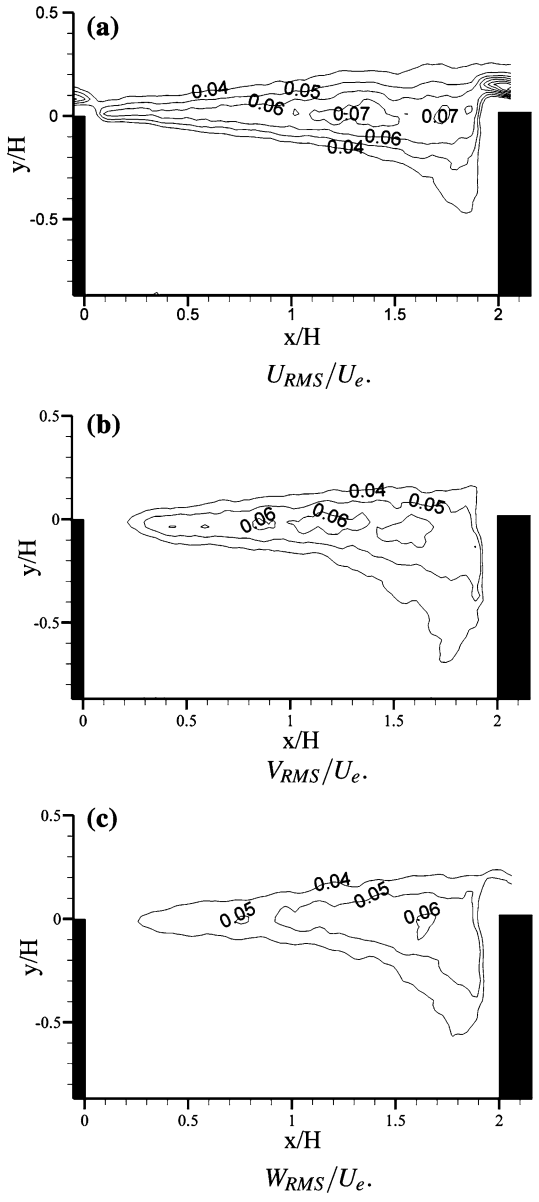


**Fig. 7** Normalized velocity RMS levels

and 0.06, respectively. Again, this location of the maxima is close to locations found in rectangular cavity flows. The maximum of the $W$-component is located more downstream at $x/H \approx 1.75$ and assumes a value of 0.06, indicating a later redistribution of turbulent kinetic energy along the spanwise direction. Moreover, the contour levels indicate an entrainment of the turbulent flow into the cavity at its trailing edge due to the asymmetric flow, a feature which is not observed for symmetric circular cavity flows.

### 4.2 Horizontal planes

In the remainder of this paper, we will denote with "left half" the area on the left side of the cavity's streamwise wall-normal plane when looking downstream where $z < 0$ located in the top of the images, whereas "right half" refers to the area on the right side of the cavity's streamwise wall-normal plane where $z > 0$. Figure 8a–d show the mean velocity field obtained from the stereo PIV measurements in the planes parallel to the wall at $y = -0.85H$,$y = -0.5H$, $y = 0$ and $y = 0.5$. In Fig. 8a a recirculation zone is observed with its center close to the upstream end. Upwards, this recirculation center is displaced in clockwise direction and disappears outside the cavity (Fig. 8b–d). The asymmetric effect propagates until approximately $y/H = 0.6$, while it is still slightly visible in Fig. 8d at $y/H = 0.5$.

Further, Fig. 9 shows that fluid enters the cavity through its "right half" downstream area and exits from it at the opposite side. This is visualized by the vertical velocity component (color code of vectors).

The 3-dimensional mean flow pattern was obtained by interpolating the mean velocity fields of the different $y$-planes obtained by stereo PIV to a 3D grid. The streamlines are calculated from two starting points at the cavity's bottom and two starting points upstream the cavity (see Fig. 10). They indicate an anticyclone like recirculation zone starting at the cavity's "right half" upstream part of the cavity bottom. It exits the cavity in the cavity's "left half" downstream area, where the center of the recirculation zone (Fig. 8c) is not visible any more due to the horizontal orientation of the vortex core line. Hence, the anticyclone is placed asymmetrically inside the cavity and it's dimension is comparable to the cavity dimensions. This result agrees with the conceptual sketch proposed by Hering et al. (2006), where the recirculation zone starts at the bottom in one half of the cavity and exits the cavity in the other half, while the core line is turned in streamwise direction as also indicated in Fig. 10. As in the studies of Hiwada et al. (1983) and Dybenko et al. (2006), also here the orientation of the asymmetric effect could be changed

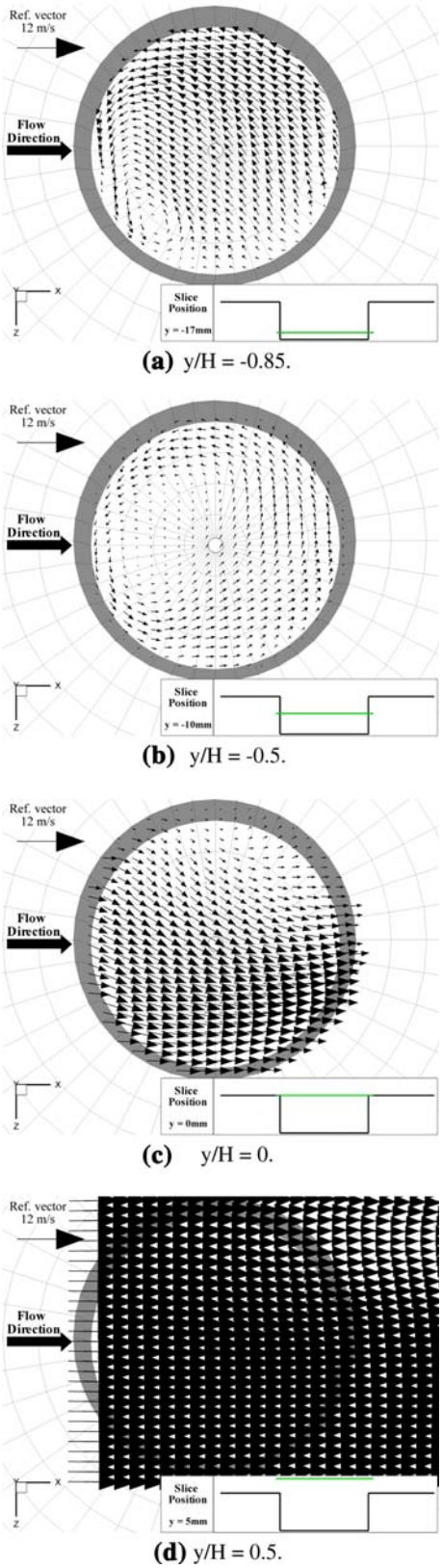


**Fig. 8** Mean velocity vector fields

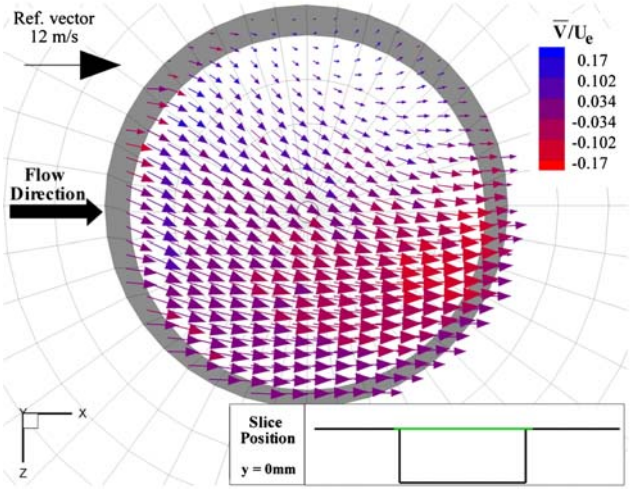


**Fig. 9** Mean velocity field at $y/H = 0$. Vector color coded by out of plane mean velocity component $\overline{V}/U_e$

by introducing a forced disturbance. Hence, it was seen to be bi-stable, where here only results for one direction of the flow asymmetry are shown. However, these results are significant for both directions as the results are just mirrored with respect to the streamwise wall-normal cavity symmetry plane.

In Figs. 11 and 12 the RMS values of the $U$ and $W$ velocity components normalized with the free stream velocity $U_e$ are shown at four different $y$-positions. Note that the contour levels are the same for the $U$ and the $W$ component, except for a few cases where a specific contour level was blanked out. The RMS values of the $V$ component are not shown here as the higher uncertainty when measuring this component with the horizontal stereo PIV setup did not allow a reliable measurement of the fluctuations.

Comparing the RMS values in the $x$–$y$-plane in the middle of the cavity (Figs. 11 and 12) with the values from Fig. 7 it is seen that similar values like in the vertical measurements are found.

Further, in the center of the recirculation zone (Fig. 11a) the RMS values are lower with respect to the outer part of the vortex. In the next higher levels (Figs. 11 and 12b, c) high turbulence activity is found close to the downstream side wall, which is due to the downwards deflection of the flow (see color code in Fig. 9). At $y = -0.15H$ (Figs. 11c and 12c) high velocity fluctuations are observed at the cavity's "right half" downstream part, where the flow is entering from the boundary layer into the cavity. Instead, at $y = 0.2H$ in Fig. 11d high values of velocity fluctuations are found where the flow exits the cavity in the cavity's "left half" downstream part and interacts with the incoming boundary layer.

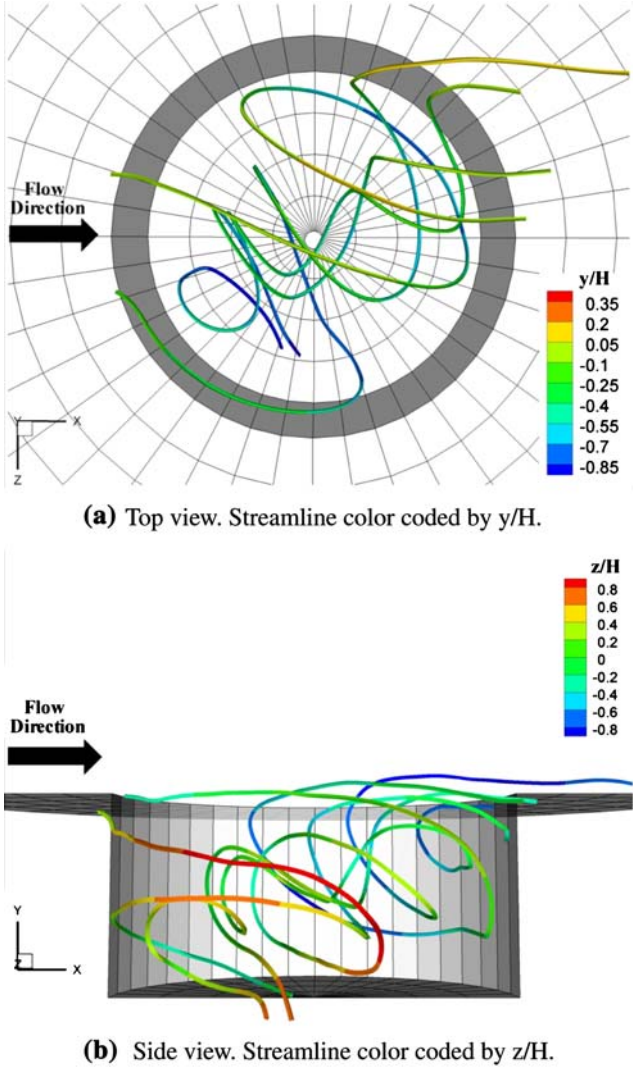


**Fig. 10** Streamlines

The here presented data cannot be compared directly with data of a circular cavity flow exhibiting a symmetric flow pattern, as such a dataset was not available to the authors. However, Dybenko et al. (2006) show, that the turbulence intensity increases in the case of an asymmetric flow pattern.

## 5 Tomographic PIV results

Figure 13 shows slices at $y = -0.15H$ through two instantaneous velocity fields obtained from the tomographic PIV measurements. The global flow pattern resembles the mean flow result shown in the stereoscopic results. However, the instantaneous fluctuations due to turbulence significantly distort the flow. The out of plane component of the velocity, coded by the vector color,

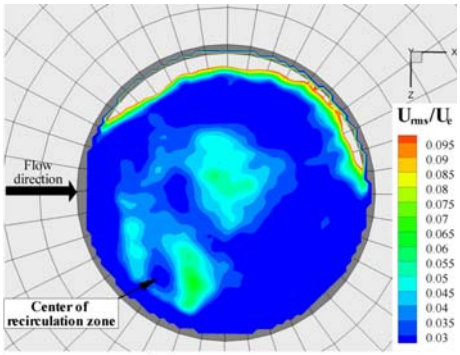


**(a)** y/H = -0.85.

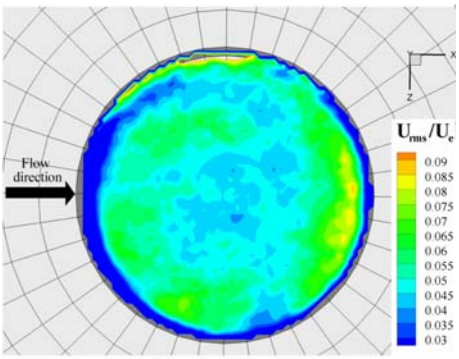


**(b)** y/H = -0.5.

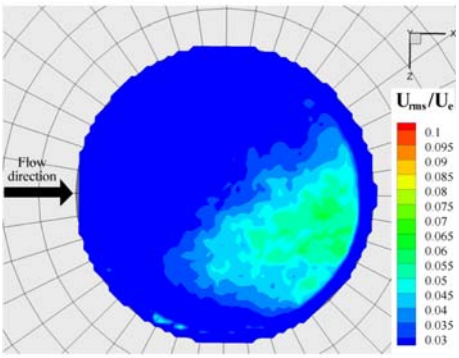


**(c)** y/H = -0.15.

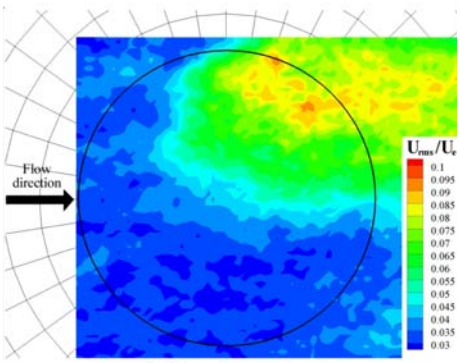


**(d)** y/H = 0.2.

**Fig. 11** The RMS values of *U*-velocity in different horizontal planes

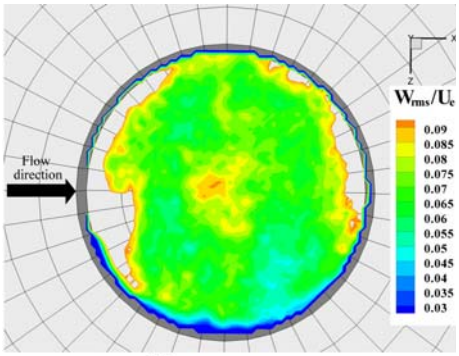


**(a)** y/H = -0.85.

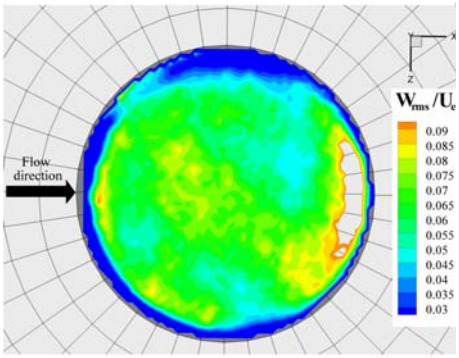


**(b)** y/H = -0.5.

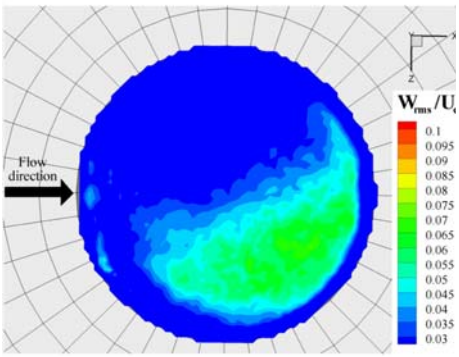


**(c)** y/H = -0.15.

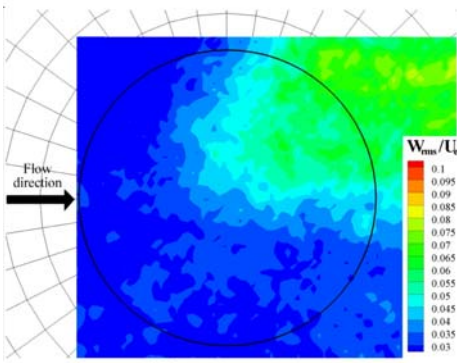


**(d)** y/H = 0.2.

**Fig. 12** The RMS values of *W*-velocity in different horizontal planes

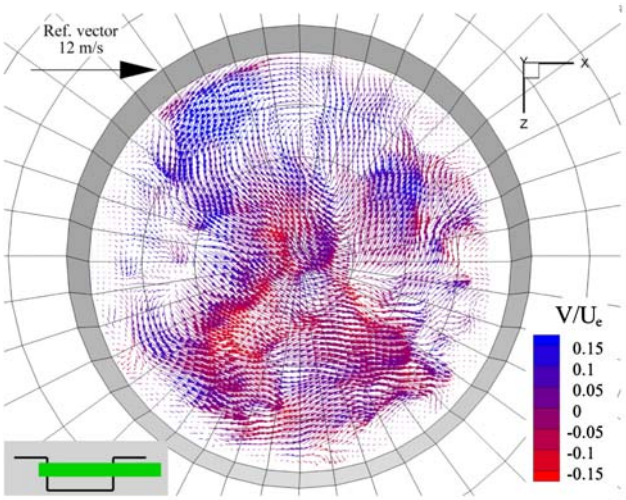


**(a)** Snapshot 1.

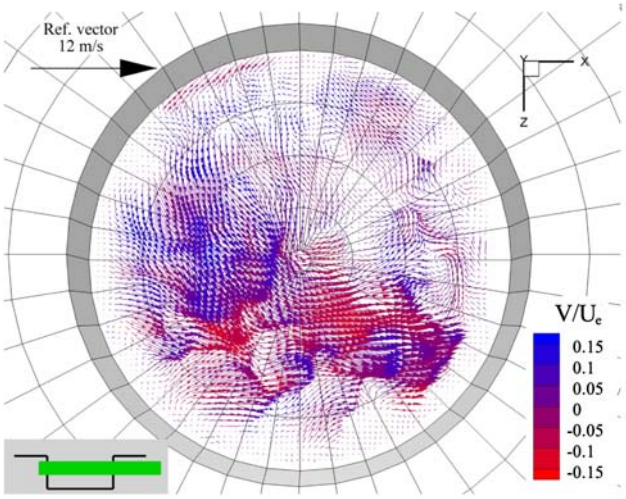


**(b)** Snapshot 2.

**Fig. 13** Slice through instantaneous velocity fields at $y/H = -0.15$

shows still the flow entering in the cavity's "right half" downstream part of the cavity and exiting at the opposite side, indicating that the asymmetric flow has a rather steady character. The flow is populated by turbulent structures, better visible in Fig. 14, where the instantaneous $\lambda_{ci}$ iso-surface are shown for $\lambda_{ci}$ = 500 l/s. One notices a higher density of vortices in the cavity's "right half", where the flow enters into the cavity. These are either vortices shed from the cavities leading edge, or structures coming from the turbulent boundary layer, which are convected inside the cavity's shear layer, but presumably it is a mixture of both effects. Instead, in the cavity's "left half", where slow fluid exits the cavity, weaker vortical structures are found. Further, an irregular distribution of vortical structures can be seen, which was also observed from the measurements in the vertical plane as described in

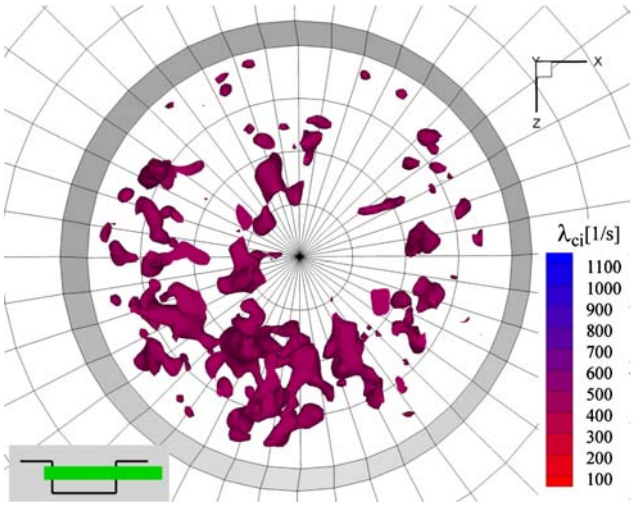


**Fig. 14** Isosurfaces of $\lambda_{ci} = 500$ l/s

Fig. 6. This indicates a more random instability mechanism in the cavity's shear layer, which is probably influenced by the turbulence properties of the thick incoming boundary layer.

## 6 Conclusion

The flow inside a circular cavity with and aspect ratio $D/H = 2$ and a fully turbulent incoming boundary layer was studied using stereoscopic and tomographic PIV.

The instantaneous velocity fields from the stereo PIV results in the vertical plane show an irregular vortex shedding from the cavity's leading edge indicated by the irregular spacing of the identified vortices. This was observed in all instantaneous vector fields. The out-of-plane component of the mean velocity field shows the asymmetrical character of the flow, where the pattern can be divided in two parts, the downstream part close to the bottom wall and the upstream part including a part of the shear layer.

The mean velocity fields at different locations parallel to the wall reveal a steady recirculation present in the cavity. Close to the bottom wall the center of the recirculation is located in the upstream part where $z > 0$. Moving further away from the bottom wall the center is displaced in clockwise direction until a position opposite to the one close to the bottom wall with respect to the cavity central axis. The streamlines indicate the form of the recirculation and show that the recirculation core line is vertical to the bottom wall for positions close to it and is tilted more and more in streamwise direction when moving out of the cavity. For planes inside the cavity, high turbulent activity is seen where the outer flow is entrained into the cavity, whereas the flow exhibits relatively low fluctuations where

it moves outwards the cavity. For planes outside the cavity, high turbulence activity is found where the flow exits the cavity and interacts with the incoming boundary layer.

The instantaneous velocity fields obtained by tomographic PIV measurements show the 3-dimensional flow pattern for an area inside the cavity. Vorticity iso-surfaces indicate flow structures which are present in the region where the flow enters the cavity, possibly shed from the cavity's leading edge or coming from the turbulent boundary layer. Stronger vortical structures are found in the cavity's "right half" ($z > 0$), where the flow enters into the cavity, whereas less strong structures are found in the cavity's "left half" ($z < 0$).

This paper was concerned with a circular cavity flow with one aspect ratio and one inflow condition. A more extensive insight into circular cavity flows could be obtained by a parametric study, changing aspect ratio and boundary layer conditions and study the influence of these changes onto the flow.

**Acknowledgments** This research project has been supported by a Marie Curie Early Stage Research Training Fellowship of the European Community's Sixth Framework Programme under contract number MEST CT 2005 020301.

## References

Dybenko J, Hering T, Savory E (2006) Turbulent boundary layer flow over circular cavities. ICAS Hamburg paper 395

Elsinga GE, Van Oudheusden BW, Scarano F (2006) Experimental assessment of tomographic-PIV accuracy. In: 13th international symposium on applications of laser techniques to fluid mechanics, paper 20.5, Lisbon, Portugal

Elsinga GE, Scarano F, Wieneke B, van Oudheusden BW (2006) Tomographic particle image velocimetry. Exp Fluids 41:933–947

Grace SM, Gary Dewar W, Wroblewski DE (2004) Experimental investigation of the flow characteristics within a shallow wall cavity for both laminar and turbulent upstream boundary layers. Exp Fluids 36:791–804

Haigermoser C, Scarano F, Onorato M (2008) 3D flow organization in rectangular cavities with laminar upstream boundary layer. 26th ICAS, paper 299

Hering T, Dybenko J, Savory E (2006) Experimental verification of CFD modeling of turbulent flow over circular cavities using FLUENT. CSME forum

Hiwada M, Kawamura T, Mabuchi I, Kumada M (1983) Some characteristics of the flow pattern and heat transfer past a circular cylindrical cavity. Bull JSME 220 26:1744–1752

Rona A (2007) The acoustic resonance of rectangular and cylindrical cavities. In: 13th AIAA/CEAS aeroacoustics conference (28th AIAA aeroacoustics conference) paper AIAA 2007–3420

Rossiter JE (1964) Wind-tunnel experiment on the flow over rectangular cavities at subsonic and transonic speeds. British ARC R&M no. 3428

Sen SN (1990) Acoustics—waves and oscillations. Wiley Eastern Ltd.

Ukeiley L, Murray N (2005) Velocity and surface pressure measurements in an open cavity. Exp Fluids 38:656–671

Wieneke B (2005) Stereo-PIV using self-calibration on particle images. Exp Fluids 39:267–280

Zou J, Adrian RJ, Balachandar S, Kendall TM (1999) Mechanisms of generating coherent packets of hairpin vortices in channel flow. J Fluid Mech 387:353–396